

Dynamic Stratified Contrastive Learning with Upstream Augmentation for MILP Branching

Tongkai Lu¹ Shuai Ma¹ Chongyang Tao¹

Abstract

Mixed Integer Linear Programming (MILP) is a fundamental class of NP-hard problems that has garnered significant attention from both academia and industry. The Branch-and-Bound (B&B) method is the dominant approach for solving MILPs and the branching plays an important role in B&B methods. Neural-based learning frameworks have recently been developed to enhance branching policies and the efficiency of solving MILPs. However, these methods still struggle with semantic variation across depths, the scarcity of upstream nodes, and the costly collection of strong branching samples. To address these issues, we propose *SC-MILP*, a Dynamic Stratified Contrastive Training Framework for MILP Branching. It groups branch-and-bound nodes based on their feature distributions and trains a GCNN-based discriminative model to progressively separate nodes across groups, learning finer-grained node representations throughout the tree. To address data scarcity and imbalance at upstream nodes, we introduce an upstream-augmented MILP derivation procedure that generates both theoretically equivalent and perturbed instances. *SC-MILP* effectively models subtle semantic differences between nodes, significantly enhancing branching accuracy and solving efficiency, particularly for upstream nodes. Extensive experiments on standard MILP benchmarks demonstrate that our method enhances branching accuracy, reduces solving time, and generalizes effectively to unseen instances.

1. Introduction

Mixed-Integer Linear Programming (MILP) constitutes a fundamental class of combinatorial optimization problems that integrates discrete and continuous decision variables

¹SKLSD Lab, Beihang University, Beijing, China. Correspondence to: Shuai Ma <shuaima@buaa.edu.cn>.

under linear constraints (Bénichou et al., 1971). It not only plays an important role in solving other combinatorial optimization problems, but also serves as a powerful modeling framework for diverse real-world applications, including cloud manufacturing, facility location, task scheduling in Web services, network design, delivery routing, and strategic planning (Zhao et al., 2025; Wang & Li, 2024; Guo et al., 2025; Floudas & Lin, 2005; Yan et al., 2024; Gao et al., 2024; Vielma, 2015; Ashouri et al., 2013; Bellabdaoui & Teghem, 2006; Soylu et al., 2006; Godart et al., 2018; Liu et al., 2023). The dominant approach for solving MILPs is the Branch-and-Bound (B&B) algorithm, an exact tree search framework that recursively partitions the feasible space into subproblems (Land & Doig, 1960). The algorithm proceeds by building a search tree where each node¹ in the B&B tree represents a subproblem defined by additional branching constraints.

In B&B, variable selection (branching) is the most critical step, as it determines which variable to branch on at each node and thereby dictates the overall structure of the search tree (Fischetti & Lodi, 2003). Consequently, the quality of branching decisions has a direct impact on both the number of nodes explored and the total solving time. Traditional variable selection methods rely heavily on expert-crafted rules and are computationally expensive, making them inflexible and time-consuming, especially for large-scale MILPs. More recently, motivated by the success of neural network methods in other combinatorial optimization domains, researchers have begun exploring their application to variable selection. Gasse et al. (2019) map the MILP problem as a bipartite graph and employs Graph Convolutional Neural Networks (GCNNs) to extract features of candidate variables for branching. It adopts an imitation learning approach, treating each node of the B&B tree as a training sample, specifically targeting strong branching (Applegate et al., 1995), which is widely adopted for generating minimal B&B trees. The study demonstrated notable performance in solving MILPs and set the trend of leveraging neural networks to improve branching strategies (Alvarez

¹In this paper, “node” refers specifically to a B&B tree node (a MILP subproblem/training instance), while “vertex” refers to a node in the MILP’s bipartite graph.

et al., 2017; Burges, 2010; Seyfi et al., 2023; Gupta et al., 2020; Zarpellon et al., 2021; Khalil et al., 2022; Lin et al., 2022; Li et al., 2025; Huang et al., 2024; Lin et al., 2024; Wang et al., 2024).

Despite progress made by current neural-based branching strategies, several critical challenges remain unsolved. First, nodes at different depths correspond to distinct solving phases, resulting in systematic semantic shifts, distributional changes, and variations in decision intent as depth increases. This continuous variation ultimately produces large disparities between upstream and downstream nodes. Nevertheless, existing neural-based branching methods (Alvarez et al., 2017; Burges, 2010; Khalil et al., 2016; Gasse et al., 2019; Gupta et al., 2020; Zarpellon et al., 2021; Lin et al., 2022; Seyfi et al., 2023; Huang et al., 2024; Lin et al., 2024; Li et al., 2025) overlook such depth-dependent differences by treating all nodes uniformly and averaging their representations, which obscures critical variations and ultimately impairs branching accuracy. Second, the inherent structural imbalance of the B&B tree yields far fewer upstream nodes than downstream ones. Consequently, training is dominated by downstream nodes, impairing performance on the critical upstream decisions that largely determine solving efficiency. Third, acquiring strong branching expert samples for imitation learning is time- and resource-intensive (Lin et al., 2024), further exacerbating the scarcity of high-quality upstream training data.

To address these challenges, we propose *SC-MILP*, a Dynamic Stratified Contrastive Training Framework for MILP Branching. Specifically, the framework groups nodes according to their feature distributions, and the GCNN-based discriminative model is trained to regulate the pairwise separation between nodes from different groups, with separation progressively increasing along the group hierarchy. This design enables the model to capture fine-grained semantic variations throughout the B&B tree. To further mitigate data scarcity and imbalance at upstream nodes, we introduce an upstream-augmented MILP derivation procedure that systematically generates both theoretically equivalent MILPs and perturbed variants from the original instances. By integrating these strategies, SC-MILP effectively captures subtle semantic differences between nodes, thereby enhancing branching accuracy, particularly for upstream nodes. The main contributions of this work are as follows:

(1) We propose *SC-MILP*, a novel training framework that initially groups nodes based on their feature distributions and subsequently trains a GCNN-based discriminative model to effectively capture semantic variation in the Branch and Bound tree.

(2) We design an *upstream-augmented MILP derivation* procedure that systematically generates both theoretically equivalent MILPs and perturbed variants from the original

instances to address data scarcity and imbalance at upstream nodes without the extra cost of collecting strong branching expert samples.

(3) We present a *dynamic stratified contrastive learning* that contrasts nodes within and across groups, with separation progressively increasing along the group hierarchy. This enables the learning of finer-grained node representations, leading to more informed and effective branching decisions.

(4) Our *SC-MILP* significantly improves MILP solving efficiency, outperforming all traditional branching strategies and neural-based methods. Moreover, it enhances branching node prediction accuracy, with particularly pronounced gains at upstream nodes.

2. Related Work

2.1. Supervised learning based methods

Supervised learning methods imitate heuristic branching rules through training predictive models. The supervised methods can be broadly categorized into those based on strong branching and those based on alternative heuristics.

Strong Branching-based Methods. Strong branching (Applegate et al., 1995) provides highly effective decisions but is computationally prohibitive. To approximate it, early works (Burges, 2010; Alvarez et al., 2017; Marcos Alvarez et al., 2014; Khalil et al., 2016) train machine learning models with strong branching labels, but with relatively low branching accuracy. Khalil et al. (2016) proposes a GCNN-based framework that represents MILPs as bipartite graphs and predicts branching scores. Building on this, FILM (Gupta et al., 2020) applies GNNs at upstream nodes and MLPs for others to enhance efficiency, TGAT (Seyfi et al., 2023) leverages temporal bipartite attention to improve branching accuracy, Chen et al. (2024) employs a second-order folklore GNN to capture complex structures but at a higher computational cost, and MILP-Evolve (Li et al., 2025) uses LLMs to generate diverse MILPs, enhancing generalization but reducing performance on individual problems. CAMBranch (Lin et al., 2024) addresses label scarcity via variable-shifting augmentation and contrastive learning between MILPs and AMILPs; however, its reliance on a single augmentation strategy limits data diversity, thereby increasing overfitting risk and hindering the model’s ability to capture complex structural and mathematical patterns.

Other Branching Strategies. TreeGate (Zarpellon et al., 2021) learns reliable pseudo-cost branching via a feature-gated DNN combining both B&B tree and variable features. Building on this, Pei & Chen (2023) employ an attention-based framework to better exploit variable interactions, MIP-GNN (Khalil et al., 2022) estimates solution quality using

variable deviations, and T-BranT (Lin et al., 2022) combines a Transformer encoder with graph attention network to capture variable features and global structure.

2.2. Reinforcement Learning based Methods

Reinforcement learning-based methods model branching as a finite-horizon Markov Decision Process (MDP). FMSTS (Etheve et al., 2020) uses deep Q-learning with subtree size as the value function. Scavuzzo et al. (2022) propose a tree-structured MDP aligned with the search tree, while Zhang et al. (2022) combine PPO with a GCNN-based value network to guide MCTS for global action optimization. Retro (Parsonson et al., 2023) converts the search tree into trajectories for efficient learning, and SORREL (Feng & Yang, 2025) leverages Self-Imitation Learning (SIL) to learn from past high-quality trajectories, improving convergence and exploration. However, reinforcement learning-based branching remains limited by sparse rewards and credit assignment, performing well only on small MILPs. Unlike the aforementioned methods that directly learn branching decisions, Symb4CO (Kuang et al., 2024a) and GS4CO (Kuang et al., 2024b) leverage reinforcement learning to “invent” a good branching algorithm and integrate symbolic learning to improve their reliability.

However, current neural methods often overlook the subtle semantic differences between nodes across depths and data scarcity at the upstream, which limits the model’s ability to learn distinct data representations necessary for accurate branching and effective MILP solving. Although a few methods, such as CAMBranch (Lin et al., 2024), acknowledge the high cost of obtaining strong branching samples, they apply uniform augmentation across all nodes, failing to address the imbalance of upstream data. Furthermore, relying on a single augmentation limits their exploitation of MILPs’ structural and mathematical properties, making the model more susceptible to overfitting. To address these limitations, we propose *SC-MILP*, a dynamic stratified contrastive training framework, which is specifically designed to capture fine-grained semantic variations across the B&B tree, thereby increasing branching accuracy and solving efficiency. To mitigate upstream data scarcity and imbalance, we introduce an upstream-augmented MILP derivation procedure, which systematically generates both theoretically equivalent MILPs and perturbed variants from the original instances. It provides greater diversity, reduces overfitting, and better exploits structural and mathematical information of MILP instances.

3. Preliminaries

Mixed Integer Linear Programming (MILP). We consider the standard form of a Mixed Integer Linear Program

(MILP), defined as follows:

$$\min_{\mathbf{x}} \mathbf{c}^T \mathbf{x} \quad \text{s.t.} \quad \mathbf{Ax} \leq \mathbf{b}, \mathbf{l} \leq \mathbf{x} \leq \mathbf{u}, x_j \in \mathbb{Z}, \forall j \in \mathcal{I}, \quad (1)$$

where $\mathbf{x} = \{x_1, \dots, x_n\} \in \mathbb{R}^{n \times n}$ is the decision variable vector, $\mathbf{c} \in \mathbb{R}^n$ is the objective coefficient vector, $\mathbf{A} \in \mathbb{R}^{q \times n}$, $\mathbf{b} \in \mathbb{R}^q$ define the system of linear inequality constraints, $\mathbf{l} \in (\mathbb{R} \cup \{-\infty\})^n$, $\mathbf{u} \in (\mathbb{R} \cup \{+\infty\})^n$ are the lower and upper bounds and $\mathcal{I} \subseteq \{1, 2, \dots, n\}$ is the index set of variables constrained to be integers.

Branching for MILPs. In a Branch-and-Bound (B&B) tree \mathcal{T} , each node s represents a subproblem with a candidate set $\text{Cand}(s)$. The goal is to learn a scoring function to evaluate the utility of branching on $x \in \text{Cand}(s)$.

$$\psi(s, x) : \mathcal{S} \times \text{Cand}(s) \rightarrow \mathbb{R}, \quad (2)$$

where \mathcal{S} denotes the set of all nodes in \mathcal{T} . The optimal branching candidate is then chosen as

$$x^*(s) = \arg \max_{x \in \text{Cand}(s)} \psi(s, x). \quad (3)$$

Bipartite Graph Representation of MILP Instances. In this paper, we follow a widely used setting in the MILP branching literature (Alvarez et al., 2017; Burges, 2010; Khalil et al., 2016; Gasse et al., 2019; Gupta et al., 2020; Zarpellon et al., 2021; Lin et al., 2022; Seyfi et al., 2023; Lin et al., 2024; Li et al., 2025), treating each node in the B&B tree as a distinct training instance for branch learning. We model each MILP instance as a bipartite graph (\mathcal{G}, C, E, V) , where \mathcal{G} encodes the bipartite structure: an edge $(i, j) \in E$ exists if variable x_j appears in constraint i . $C \in \mathbb{R}^{|C| \times d_1}$ and $V \in \mathbb{R}^{|V| \times d_2}$ store constraint and variable vertex features, respectively, and $E \in \mathbb{R}^{|C| \times |V| \times d_3}$ represents edge features. The details of these features are summarized in Appendix D.1.

4. Method

4.1. Overview

In this section, we present *SC-MILP*, a dynamic stratified contrastive training framework designed for accurate branching and efficient MILP solving, with an overview shown in Fig. 1. We first introduce stratified node grouping to partition nodes into feature-driven strata, capturing continuous structural and solving-stage variations for subsequent steps. To address upstream scarcity and imbalance, we then employ upstream-augmented MILP derivation, generating both theoretically equivalent MILPs (via linear transformations of variables and constraints) and perturbed MILPs (lightweight perturbations applied to objectives, constraints, and dual variables), without incurring additional data collection overhead, while simultaneously enriching the training distribution. Finally, we apply dynamic stratified contrastive learning to leverage semantic and feature variations across the tree, thereby improving node representations and branch-

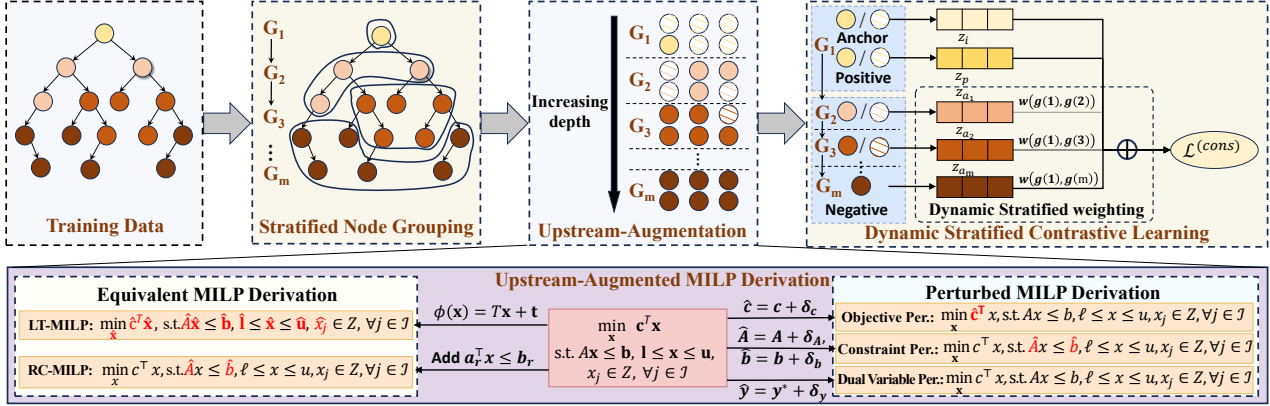


Figure 1. Overview of our SC-MILP. Each node in the B&B tree is color-coded to reflect feature variations across depths, while nodes marked with slashes denote additional samples generated via upstream-augmented MILP derivation. Nodes are first grouped into feature-driven strata (G_1, G_2, \dots). Both equivalent and perturbed MILP derivations are then applied to augment upstream samples. Specifically, LT-MILP and RC-MILP refer to derivations based on linear transformation and redundant constraint generation, respectively, whereas objective Per., constraint Per., and dual variable Per. indicate perturbations applied to the objective, constraints, and dual variables. Finally, dynamic stratified contrastive learning is performed, where positives are defined within the same stratum and negatives across different strata, with dynamic stratified weighting that progressively increases separation with group depth and is adaptively modulated during training.

ing accuracy. Formally, for each anchor node, nodes within the same group are treated as positives, while nodes from other groups are treated as negatives. We compute pairwise similarities between the anchor node and all other nodes, where dynamic stratified weights are applied to rescale the similarities based on group depth differences. This dynamic stratified contrastive loss progressively preserves intra-group consistency, promotes moderate separation between adjacent strata, and enforces stronger discrimination across distant strata, leading to more informed and effective branching decisions.

4.2. Stratified Node Grouping

Considering that nodes at similar depths share comparable solving contexts, we perform *stratified node grouping* that partitions nodes into different strata based on their feature distributions, thereby capturing structural and semantic variations across the B&B tree and providing fine-grained contextual information for dynamic stratified contrastive learning.

Formally, we partition the node set into m groups, $\{G_1, \dots, G_m\}$, using unsupervised clustering (e.g., K-means²) based on node features, with the number of groups m determined via the elbow method. This principled grouping establishes a clear stratification that underpins subsequent upstream-augmented MILP derivation and dynamic stratified contrastive learning.

²We adopt K-means as it provides a simple yet effective solution for our task; alternative clustering methods did not yield additional benefits in our experiments.

4.3. Upstream-Augmented MILP Derivation

Due to the structural imbalance of the B&B tree, the number of nodes varies significantly across depth, with upstream nodes typically fewer than downstream nodes. This imbalance can negatively impact subsequent dynamic stratified contrastive learning, as the scarcity of upstream nodes limits the model’s ability to capture semantic features at early stages, thereby reducing its discriminative power on critical nodes. After stratified node grouping, the original imbalance becomes more pronounced, appearing as a marked disparity in node counts across groups. A natural solution is to regenerate strong branching expert samples to supplement underrepresented groups. However, this strategy faces two key challenges: (1) generating a sufficient number of samples is computationally expensive, and (2) the newly generated nodes may not faithfully preserve the feature distribution of the original groups, potentially impairing model learning.

To address these issues, we propose an *upstream-augmented MILP derivation* approach that systematically derives new training samples from the original MILP problems rather than relying on additional data collection. Specifically, the equivalence-based derivation applies linear transformations and combinations to produce formally distinct yet equivalent samples in terms of feasible regions and strong branching labels, while the perturbation-based derivation introduces slight modifications to constraints and dual variables to enhance generalization and robustness. Unlike ordinary data augmentation, our method constitutes a strict derivation grounded in the structural properties of the original MILPs with a theoretical foundation and establishes the correspondence between augmented and original bipartite graphs in

Appendix D, thereby ensuring both fidelity and soundness.

4.3.1. EQUIVALENT MILP DERIVATION

Intuitively, our goal is to enrich upstream training data without altering the underlying MILP problems. To this end, we leverage the expert knowledge embedded in the original MILPs and introduce two equivalent MILP derivation methods: the linear transformation based derivation (*LT-MILP*, Definition 1) and the redundant constraint based derivation (*RC-MILP*, Definition 2). Each method is rigorously justified through theoretical guarantees (Theorems 4.2, 4.3, and 4.4) with formal proofs provided in Appendix C. These ensure a one-to-one correspondence between the feasible regions (including integer variables) of the original and augmented MILPs, as well as between their strong branching outcomes, thereby preserving both fidelity and theoretical rigor.

Definition 4.1 (Linear transformation based Equivalent MILP Derivation (*LT-MILP*)). Given an MILP problem in Equ. 1, let $\phi(\mathbf{x}) = T\mathbf{x} + \mathbf{t}$ be an affine transformation, where T is a special diagonal matrix whose diagonal entries are either 1 or -1 ($T^{-1} = T$) and $\mathbf{t}_\mathcal{I} \in \mathbb{Z}^k$. This linear transformation $\phi(\cdot)$ leads to an equivalent new MILP problem:

$$\min_{\hat{\mathbf{x}}} \hat{\mathbf{c}}^\top \hat{\mathbf{x}} \quad \text{s.t.} \quad \hat{A}\hat{\mathbf{x}} \leq \hat{\mathbf{b}}, \hat{\mathbf{l}} \leq \hat{\mathbf{x}} \leq \hat{\mathbf{u}}, \hat{x}_j \in \mathbb{Z}, \forall j \in \mathcal{I} \quad (4)$$

where $\hat{\mathbf{c}} = T\mathbf{c}$ is the transformed objective coefficient vector, $\hat{A} = AT$ is the transformed constraint matrix, $\hat{\mathbf{b}} = \mathbf{b} + ATT\mathbf{t}$ and the left and right bounds $\hat{\mathbf{l}} = T\mathbf{l} + \mathbf{t}$, $\hat{\mathbf{u}} = T\mathbf{u} + \mathbf{t}$.

Next, we present three theorems establishing the equivalence between *LT-MILP* and the original MILP problem, with proofs given in Appendix C.

Theorem 4.2. Let $\mathcal{P} := \{ \mathbf{x} \in \mathbb{R}^n \mid A\mathbf{x} \leq \mathbf{b}, \mathbf{l} \leq \mathbf{x} \leq \mathbf{u} \}$ be the feasible region of the LP relaxation of Eq. 1, and let $\hat{\mathcal{P}} := \{ \hat{\mathbf{x}} \in \mathbb{R}^n \mid \hat{A}\hat{\mathbf{x}} \leq \hat{\mathbf{b}}, \hat{\mathbf{l}} \leq \hat{\mathbf{x}} \leq \hat{\mathbf{u}} \}$ be the feasible region of the LP relaxation of Eq. 4. Then: (1) The affine transformation $\phi(\cdot)$ is a bijection between \mathcal{P} and $\hat{\mathcal{P}}$, i.e., the LP feasible domains are in one-to-one correspondence. (2) This bijection $\phi(\cdot)$ induces a one-to-one correspondence between the sets of optimal solutions of the two LPs.

Theorem 4.3. For any variable x_j in the original problem of Equ. 1, the strong branching decisions correspond exactly to those of $\hat{x}_{\pi(j)}$ in the transformed problem of Equ. 4, where π is the variable mapping induced by $\phi(\cdot)$.

Theorems 4.2 and 4.3 together establish the equivalence between the original and the transformed problems in terms of feasible regions and strong branching outcomes. To further broaden the theoretical scope and provide more diverse and complex augmented MILPs, we generalize the linear transformation assumption to a more flexible class of affine mappings in the following theorem.

Theorem 4.4. Let the index set of integer variables in Eq. 1 be $\mathcal{I} = \{1, 2, \dots, k\}$, and partition vectors and matrices conformably so that

$$\mathbf{x} = (\mathbf{x}_\mathcal{I}^T, \mathbf{x}_\mathcal{F}^T)^T, \quad \mathbf{x}_\mathcal{I} \in \mathbb{Z}^k, \quad \mathbf{x}_\mathcal{F} \in \mathbb{R}^{n-k}.$$

Assume the transformation matrix

$$T = \begin{pmatrix} B & 0 \\ F & D \end{pmatrix},$$

where the blocks and the translation vector $\mathbf{t} = (\mathbf{t}_\mathcal{I}^T, \mathbf{t}_\mathcal{F}^T)^T$ satisfy: (a) $B \in \mathbb{R}^{k \times k}$ is a signed permutation matrix (thus each row and column has exactly one entry equal to ± 1 and all others are zero. Hence B is invertible and $B^{-1} = B^\top$ with integer entries); (b) $F \in \mathbb{R}^{(n-k) \times k}$ and $D \in \mathbb{R}^{(n-k) \times (n-k)}$ with D invertible; (c) $\mathbf{t}_\mathcal{I} \in \mathbb{Z}^k$. Then we have that (1) The affine map $\phi(\mathbf{x}) = T\mathbf{x} + \mathbf{t}$ is a bijection between the feasible region of the original MILP and that of the transformed MILP, and it preserves the integrality of the integer components: if $\mathbf{x}_\mathcal{I} \in \mathbb{Z}^k$ then $\hat{\mathbf{x}}_\mathcal{I} = B\mathbf{x}_\mathcal{I} + \mathbf{t}_\mathcal{I} \in \mathbb{Z}^k$, and conversely. (2) The bijection ϕ induces a one-to-one correspondence between optimal solutions of the two MILPs (and of their LP relaxations).

Remark. Theorem 4.4 shows that the equivalence between the original and transformed MILPs holds under a broader class of linear transformations, far beyond the specific cases considered in Definition 1. In this paper, we only adopt the simpler transformation forms from Definition 1, as they are easier to implement and already provide sufficient diversity for current benchmarks.

Definition 4.5 (Redundant Constraint based Equivalent MILP Derivation (*RC-MILP*)). Given an MILP problem in Eq. 1, let $a_i^\top \mathbf{x} \leq b_i$ and $a_j^\top \mathbf{x} \leq b_j$ be two linearly independent constraints; define a new redundant constraint $a_r^\top \mathbf{x} \leq b_r$ with $a_r = a_i + a_j$, $b_r = b_i + b_j$. Augmenting the MILP with this constraint yields $\min_x \mathbf{c}^\top \mathbf{x}$ s.t. $\hat{A}\hat{\mathbf{x}} \leq \hat{\mathbf{b}}, \mathbf{l} \leq \mathbf{x} \leq \mathbf{u}, x_j \in \mathbb{Z}, \forall j \in \mathcal{I}$, where $\hat{A} = \begin{bmatrix} A & 0 \\ a_r^\top & b_r \end{bmatrix}, \hat{\mathbf{b}} = \begin{bmatrix} \mathbf{b} \\ b_r \end{bmatrix}$.

As the constraints of *RC-MILP* are essentially equivalent to those of the original problem, their LP relaxations share exactly the same feasible region. Consequently, they produce identical strong branching results and optimal solutions. Therefore, *RC-MILP* serves as an equivalent derivation of the original MILP.

4.3.2. PERTURBED MILP DERIVATION

Equivalent sample derivation ensures strict preservation of feasible regions and strong branching outcomes, providing reliable samples for training. To complement this approach and expose the model to a broader variety of problem structures, we introduce a perturbation-based derivation method

that generates non-identical MILPs by applying small perturbations to objective coefficients, constraint coefficients, or dual variables. Although these perturbations may slightly alter the branching outcomes, we retain the original strong branching outcomes during training to encourage the model to learn more resilient representations. Specifically, we consider three types of perturbations: objective perturbation, constraint perturbation, and dual variable perturbation, shown in Definition 3 & 4.

Definition 4.6 (Objective and Constraint Perturbation). Given an MILP in standard form, we consider two types of perturbations to generate derived MILPs:

(1) Objective Perturbation: The objective vector is perturbed as $\hat{\mathbf{c}} = \mathbf{c} + \delta_c$, where $\delta_c \in \mathbb{R}^n$ is a small perturbation sampled from a Gaussian distribution. The augmented MILP becomes

$$\min_{\mathbf{x}} \hat{\mathbf{c}}^T \mathbf{x} \quad \text{s.t.} \quad A\mathbf{x} \leq \mathbf{b}, \quad 1 \leq \mathbf{x} \leq \mathbf{u}, \quad x_j \in \mathbb{Z}, \quad \forall j \in \mathcal{I}$$

(2) Constraint Perturbation: The constraint system is perturbed as $\hat{A} = A + \delta_A$, $\hat{\mathbf{b}} = \mathbf{b} + \delta_b$, where $\delta_A \in \mathbb{R}^{q \times n}$ and $\delta_b \in \mathbb{R}^q$ are small perturbations sampled from Gaussian distributions. The augmented MILP is

$$\min_{\mathbf{x}} \mathbf{c}^T \mathbf{x} \quad \text{s.t.} \quad \hat{A}\mathbf{x} \leq \hat{\mathbf{b}}, \quad 1 \leq \mathbf{x} \leq \mathbf{u}, \quad x_j \in \mathbb{Z}, \quad \forall j \in \mathcal{I}$$

Definition 4.7 (Dual Variable Perturbation). For the LP relaxation of the MILP, let $y^* \in \mathbb{R}^m$ denote the optimal dual variables corresponding to constraints $Ax \leq b$. To enhance robustness to solver sensitivity and numerical instability, we perturb the dual variables by injecting Gaussian noise δ_y

$$\hat{y} = y^* + \delta_y,$$

4.4. Dynamic Stratified Contrastive Learning

In the Branch-and-Bound (B&B) tree for solving MILPs, node feature distributions vary significantly across depths. For example, `sol_is_at_lb` (`sol_is_at_ub`)—indicating whether a variable’s LP solution matches its lower (upper) bound—is typically zero for upstream nodes but mostly one for downstream nodes, where many variables are already fixed. These differences arise because nodes at different depths represent different solving phases: upstream nodes capture global optimization potential, whereas downstream nodes are strongly shaped by prior branching decisions. Learning a single shared representation thus dilutes critical upstream signals, reducing both branching accuracy and generalization.

A natural alternative is supervised contrastive learning (SCL) (Khosla et al., 2020), where nodes from the same group are pulled together and all others are treated as negatives. While SCL captures intra-group similarity, it overlooks the gradual semantic variation across depths. In particular, nodes from adjacent groups—though semantically

close—are pushed apart as strongly as distant ones. This abrupt separation neglects the progressive, stratified nature of node semantics, degrading representation quality and limiting branching accuracy, especially for the critical yet underrepresented upstream nodes.

To address these issues, we propose a *dynamic stratified contrastive learning framework*, which explicitly leverages semantic and feature variations across the B&B tree. Unlike conventional SCL, which treats all negatives uniformly, our framework introduces a dynamic stratified weighting mechanism that weights positive and negative node pairs according to their depth distance: nearby nodes are kept moderately close, while distant nodes are strongly separated. This stratified weighting strategy preserves intra-group consistency, encourages gradual separation across adjacent phases, and enforces stronger discrimination for distant phases, improving the node representations’ quality for branching decisions.

We initiate the process with node i (an MILP sample) and its bipartite graph $s_i = (\mathcal{G}_i, C_i, E_i, V_i)$. Then s_i is fed into a Graph Convolutional Neural Network (GCNN)³ for message passing between variable and constraint vertices, obtaining the variable representations $Z_i = \{z_v \mid v \in V_i\}$ for the entire graph. For a mini-batch containing multiple problem instances s_i , we collect all node embeddings from their respective graphs to construct a unified representation pool, enabling cross-instance contrastive learning. Based on these embeddings, we next introduce both *dynamic stratified contrastive loss* that encourages gradual separation across adjacent groups and the supervised loss for learning branching decisions.

Formally, the dynamic stratified contrastive loss is defined as:

$$\mathcal{L}^{(cons)} = \sum_i -\frac{1}{|P(i)|} \sum_{p \in P(i)} \log \frac{\exp(\text{sim}(Z_i, Z_p) / \tau)}{\text{sum}_A}, \quad (5)$$

where $\text{sum}_A = \sum_{j \in A(i)} \exp(w(g(i), g(j)) \cdot \text{sim}(Z_i, Z_j) / \tau)$, s_i denotes the anchor node, $g(i)$ returns the group index of node s_i , $P(i) = \{p \neq i \mid g(p) = g(i)\}$ is the index set of positive nodes in the same group, $A(i) = \{a \neq i\}$ denotes all other nodes, and $\text{sim}(\cdot, \cdot)$ is the cosine similarity.

The *dynamic stratified weight* is defined to control the separation strength between nodes from different groups, as follows

$$w(g(i), g(j)) = \sigma(\alpha_{|g(i)-g(j)|}), \quad (6)$$

where $\sigma(\cdot)$ is the sigmoid function that bounds the weight within $(0, 1)$ for training stability, α_k is a non-decreasing

³We adopt the standard GCNN, which remains widely used due to its strong performance and fast inference speed. Compared with more complex models such as GAT, GCNN enables faster branching decisions, resulting in higher overall efficiency.

function of the group distance, parameterized as

$$\alpha_k = \sum_{j=1}^k \beta_j, \quad \beta_j = \text{softplus}(\theta_j) \geq 0, (\alpha_0 = 1) \quad (7)$$

where θ_j are learnable parameters and $\text{softplus}(x) = \log(1 + e^x)$ ensures positivity for monotonicity and enables backpropagation. This formulation preserves intra-group consistency and enforces moderate separation between adjacent groups, while dynamically weighting pairwise similarities such that larger weights induce stronger separation and smaller weights reduce their influence.

In addition, to enable the model to learn strong branching decisions, we adopt a commonly used supervised loss based on cross-entropy. Specifically, the variable representations Z_i of the entire graph are fed into a multilayer perceptron layer (MLP) to predict a branching score for each candidate variable $v \in V_i$, and the highest-scoring variable a_i is selected during inference. The network is then optimized using the cross-entropy loss

$$\mathcal{L}^{(\text{sup})} = -\frac{1}{N} \sum_{(s, a) \in \mathcal{D}} \log \pi_{\theta}(a_i^* | s_i). \quad (8)$$

where a_i^* is the branch decision of strong branching under s_i , \mathcal{D} is the training sets, $N = |\mathcal{D}|$ and θ_{sup} is the parameters of the GCNN.

The overall training objective combines the original supervised loss $\mathcal{L}^{(\text{sup})}$ with the dynamic stratified contrastive loss:

$$\mathcal{L} = \mathcal{L}^{(\text{sup})} + \lambda \mathcal{L}^{(\text{cons})}, \quad (9)$$

where λ is a learnable parameter as a balancing coefficient, set to 0 during inference.

4.5. Branching with SC-MILP

During MILP solving, SC-MILP can be invoked at every B&B branching decision. At upstream nodes near the root, where branching largely determines search time and tree size, we adopt a hybrid strategy: SC-MILP first predicts scores for all candidate variables to identify the top-k, and strong branching selects the highest-scoring one. Downstream nodes, in contrast, directly use SC-MILP for branching.

Since the total depth of the B&B tree is unknown, we use candidate set size to distinguish upstream from downstream nodes, reflecting both solving stage and branching difficulty: shallow nodes have larger, more ambiguous candidate sets, whereas deeper nodes have smaller, more constrained and informative ones. The threshold d_0 is set as the shallowest depth where a node's candidate set is no more than a fraction ρ of all variables, *i.e.*,

$$d_0 = \min \{d \mid n_{\text{cand}}(d) \leq \rho \cdot n_{\text{root}}\},$$

where $n_{\text{cand}}(d)$ is the number of branching candidates at depth d , and variable ratio threshold $\rho \in (0, 1)$ is a hyperparameter distinguishing upstream and downstream nodes.

5. Experiments

5.1. Experimental Settings

Datasets. We evaluate our method on four NP-hard benchmarks widely used in prior work (Alvarez et al., 2017; Burges, 2010; Khalil et al., 2016; Gasse et al., 2019; Gupta et al., 2020; Zarpellon et al., 2021; Lin et al., 2022; Seyfi et al., 2023; Lin et al., 2024; Li et al., 2025), including Set Covering (Balas & Ho, 2009), Combinatorial Auction (Leyton-Brown et al., 2000), Capacitated Facility Location (Cornuéjols et al., 1991), and Maximum Independent Set (Bergman et al., 2016). All instances are collected from SCIP rollouts with Strong Branching and provided at three difficulty levels (Easy, Medium, Hard), with training sets on the easy level using 100K expert samples and testing on all three levels with 100 instances each. We conduct all experiments using SCIP 7.0.1⁴ as the backend solver with a one-hour time limit.

Baselines. We compare our algorithm against a range of B&B branching methods: (1) conventional methods full strong branching (FSB) (Applegate et al., 1995) and Reliability Pseudocost Branching (RPB) (Achterberg et al., 2005), (2) machine learning based methods Trees (Alvarez et al., 2017), LMART (Burges, 2010) and svmrk (Khalil et al., 2016), (3) neural based methods GCNN (Gasse et al., 2019), FILM (Gupta et al., 2020), TreeGate (Zarpellon et al., 2021), T-BranT (Lin et al., 2022), TGAT (Seyfi et al., 2023), CAM-Branch (Lin et al., 2024), MILP-Evolve (Li et al., 2025), and (4) RL based methods Symb4CO (Kuang et al., 2024a) and GS4CO (Kuang et al., 2024b).

Metrics. Following standard MILP benchmarks, we evaluate solving time (time), the number of nodes in the B&B tree (nodes), and the number of times each method achieves the best solving time (wins), where lower time and nodes are better, and higher wins are preferred, with solving time being most important. To assess branching decisions, we report top-k accuracy (acc@1, acc@3, acc@5, acc@10), indicating the fraction of samples where the variable selected by the strong branching is among the top-k variables.

Parameter Setting. According to the elbow methods, the group number m for stratified node grouping is set to 4 (Set Covering, Combinatorial Auction, Maximum Independent Set) and 5 (Capacitated Facility Location). Upstream augmentation applies two equivalent MILP derivations with

⁴Some baseline implementations originally used either SCIP 6.0.1 or 7.0.1. For consistency, we standardize all experiments on SCIP 7.0.1, which ensures reproducibility and fair comparison across methods.

Table 1. Policy evaluation in terms of solving time, number of B&B nodes, and number of wins over number of solved instances on four combinatorial optimization problems. The best-performing methods in terms of Wins and Time are highlighted in bold, while for Nodes, the best neural-based method is highlighted.

Model	Set Covering									Combinatorial Auction								
	Easy			Medium			Hard			Easy			Medium			Hard		
	Wins↑	Time↓	Nodes↓	Wins↑	Time↓	Nodes↓	Wins↑	Time↓	Nodes↓	Wins↑	Time↓	Nodes↓	Wins↑	Time↓	Nodes↓	Wins↑	Time↓	Nodes↓
FSB (Applegate et al., 1995)	0/100	17.42	16	0/100	409.32	164	0/100	3600	n/a	0/100	4.12	6	0/100	87.45	72	0/100	1821.62	401
RPB (Achterberg et al., 2005)	0/100	8.91	55	0/100	59.73	1734	0/100	1654.84	47352	0/100	2.73	10	0/100	21.87	687	0/100	137.11	5472
Trees (Alvarez et al., 2017)	0/100	9.31	187	0/100	92.66	4203	0/100	1800.62	45126	0/100	2.51	87	0/100	23.66	980	0/100	458.35	10183
LMART (Burges, 2010)	0/100	7.21	171	0/100	59.86	1903	0/100	1252.01	34331	0/100	1.98	75	11/100	17.42	876	0/100	224.02	6149
svmrk (Khalil et al., 2016)	0/100	8.07	163	0/100	73.06	1937	4/100	1038.14	31089	0/100	2.34	78	0/100	23.16	868	0/100	376.61	6816
GCNN (Gasse et al., 2019)	11/100	6.11	171	4/100	42.44	1484	0/100	1299.99	37108	0/100	1.88	72	0/100	19.31	655	1/100	114.32	5231
FILM (Gupta et al., 2020)	3/100	6.29	165	0/100	44.32	1391	0/100	1392.42	33692	11/100	1.77	73	0/100	26.04	857	0/100	416.53	5310
TreeGate (Zarpellon et al., 2021)	0/100	8.32	231	0/100	51.4	2410	0/100	2085.85	58536	0/100	2.35	83	0/100	18.32	862	0/100	176.4	5437
T-BranT (Lin et al., 2022)	0/100	6.91	153	0/100	43.53	1653	0/100	1154.46	34694	0/100	2.28	89	0/100	19.56	723	0/100	142.73	6742
TGAT (Seyfi et al., 2023)	3/100	6.8	127	1/100	46.81	1336	1/100	1174.38	29452	0/100	2.01	75	3/100	22.03	694	0/100	126.49	5531
Symb4CO (Kuang et al., 2024a)	19/100	6.09	151	4/100	43.37	1438	0/100	1372.47	57315	29/100	1.69	75	5/100	17.34	743	4/100	108.7	5637
GS4CO (Kuang et al., 2024b)	2/100	6.21	216	3/100	42.74	1735	2/100	1147.84	63142	10/100	1.73	82	1/100	18.48	746	3/100	104.39	6482
CAMBranch (Lin et al., 2024)	2/100	6.33	139	11/100	41.53	1279	4/100	1104.34	31584	4/100	1.77	87	3/100	17.79	683	0/100	125.94	4904
MILP-Evolve (Li et al., 2025)	0/100	10.31	144	3/100	46.37	1431	7/100	1024.21	30812	3/100	1.78	64	12/100	17.5	663	5/100	106.73	5316
Ours	60/100	5.99	117	74/100	37.01	1452	82/100	953.24	29375	53/100	1.63	68	65/100	16.85	645	87/100	99.81	4721
Model	Capacitated Facility Location									Maximum Independent Set								
	Easy			Medium			Hard			Easy			Medium			Hard		
	Wins↑	Time↓	Nodes↓	Wins↑	Time↓	Nodes↓	Wins↑	Time↓	Nodes↓	Wins↑	Time↓	Nodes↓	Wins↑	Time↓	Nodes↓	Wins↑	Time↓	Nodes↓
FSB (Applegate et al., 1995)	0/100	30.49	14	0/100	224.13	81	0/100	748.33	52	0/100	23.57	7	0/100	1581.86	38	0/100	3600	n/a
RPB (Achterberg et al., 2005)	0/100	26.37	23	0/100	157.73	169	0/100	645.72	105	0/100	11.33	21	0/100	111.41	731	0/100	2124.75	7815
Trees (Alvarez et al., 2017)	0/100	28.91	133	0/100	159.88	404	0/100	634.12	400	0/100	10.68	73	0/100	1178.31	4643	0/100	3442.23	28210
LMART (Burges, 2010)	0/100	23.36	114	0/100	129.1	357	0/100	520.26	345	14/100	8.31	52	0/100	219.22	747	0/100	3356.55	33732
svmrk (Khalil et al., 2016)	0/100	23.61	116	0/100	130.88	351	0/100	512.98	331	0/100	13.77	45	0/100	241.83	541	0/100	3174.23	20030
GCNN (Gasse et al., 2019)	0/100	22.15	107	0/100	121.31	341	0/100	563.54	345	0/100	11.44	43	0/100	192.86	1837	0/100	1187.5	18668
FILM (Gupta et al., 2020)	0/100	21.56	104	1/100	116.81	337	0/100	543.14	358	0/100	10.73	47	0/100	164.57	1682	0/100	3528.71	16667
TreeGate (Zarpellon et al., 2021)	0/100	21.57	126	0/100	126.8	456	0/100	929.82	495	0/100	11.86	56	0/100	131.3	1732	0/100	3338.97	16596
T-BranT (Lin et al., 2022)	0/100	18.62	142	0/100	135.22	1052	0/100	638.19	1220	0/100	9.31	51	0/100	113.44	1521	0/100	3338.47	7011
TGAT (Seyfi et al., 2023)	15/100	17.92	96	4/100	113.12	299	3/100	372.71	336	5/100	8.45	46	17/100	96.42	1457	0/100	1201.55	18442
Symb4CO (Kuang et al., 2024a)	0/100	19.94	121	14/100	109.66	313	0/100	497.39	338	0/100	10.8	49	0/100	134.72	794	9/100	1095.41	17837
GS4CO (Kuang et al., 2024b)	0/100	22.72	101	0/100	119.83	327	0/100	452.83	345	0/100	10.53	52	0/100	131.35	852	1/100	1137.28	16341
CAMBranch (Lin et al., 2024)	9/100	18.11	97	2/100	114.53	317	0/100	461.83	359	2/100	9.07	41	0/100	145.09	1648	3/100	1143.61	16473
MILP-Evolve (Li et al., 2025)	2/100	20.58	103	0/100	117.65	327	5/100	352.5	324	2/100	8.79	48	0/100	135.7	1586	0/100	1163.47	17663
Ours	74/100	17.14	111	79/100	104.38	309	92/100	331.3	294	77/100	7.89	44	83/100	94.1	1385	87/100	964.79	14726

35% probability and three perturbed derivations with 10% to maintain stability and reliability of upstream samples. Based on the experimental results in Exp-4, the temperature τ for dynamic stratified contrastive learning is set to 0.08, the hybrid branching ratio ρ is set to 0.8 and $k = 5$ since *SC-MILP* achieves over 90% acc@5 (Table 2). The training set follows the standard configuration in prior works (Khosla et al., 2020; Gasse et al., 2019; Gupta et al., 2020; Zarpellon et al., 2021; Lin et al., 2024), and all baselines use their released code with default parameters.

5.2. Experimental Results

Exp-1: Overall Comparison with Existing Methods. We first compare our method with baseline methods on four different datasets. The results are presented in Table 1. Our *SC-MILP* consistently outperforms all baseline methods in terms of solving time and number of wins, while also generating fewer B&B nodes in most cases.

Solving time is the most direct indicator of the performance of a branching policy. *SC-MILP* achieves the shortest solving time across all datasets, improving efficiency by 12.36% on average over the current SOTA MILP-Evolve and by 26.48% over GCNN. On easy, medium, and hard instances, the gains over MILP-Evolve reach 21.25%, 20.45%, and 11.25%, respectively. Notably, almost all neural-based methods surpass the traditional FSB and RPB, highlighting the

effectiveness of neural-based branching strategies.

The B&B tree size directly reflects space usage and generally correlates with solving efficiency. On average, *SC-MILP* explores 3.28% fewer nodes than T-BranT, the best-performing baseline in terms of nodes, and 26.48% fewer than MILP-Evolve, reflecting a substantial improvement in search efficiency and pruning effectiveness. While occasionally generating more nodes, it still achieves the least solving time, as efficiency depends on both node count and per-node computation. T-BranT’s attention modules slow per-node inference, while our method adopts a hybrid branching strategy, which refines branching decisions with minimal overhead. Additionally, traditional methods like FSB and RPB may produce fewer nodes but remain less efficient due to costly branching decisions.

The number of wins measures how often a method achieves the shortest solving time among all competitors. Our method achieves the best result in 77.08% of instances, significantly higher than all baselines. Breaking this down by difficulty, our approach wins on 66.00% of easy, 75.25% of medium, and 87.00% of hard instances. The performance gap becomes larger as the problem difficulty increases, suggesting that our method generalizes better to large and challenging instances beyond the training distribution.

Overall, *SC-MILP* reduces solving time and tree size while

Table 2. Imitation learning accuracy on the test sets (%).

Model	Set Covering			Combinatorial Auction			Capacitated Facility Location			Maximum Independent Set		
	acc@1↑	acc@3↑	acc@5↑	acc@10↑	acc@1↑	acc@3↑	acc@5↑	acc@10↑	acc@1↑	acc@3↑	acc@5↑	acc@10↑
Trees (Alvarez et al., 2017)	54.7	74.9	83.7	93.3	47.7	69.6	80.1	91.5	63.4	90.0	96.7	99.9
LMART (Burges, 2010)	60.1	78.4	86.3	94.8	48.8	69.1	79.3	90.3	68.3	92.4	97.2	99.9
svmrnk (Khalil et al., 2016)	59.9	79.1	86.3	95.0	58.0	77.6	86.2	94.0	68.2	92.0	97.5	100.0
GCNN (Gasse et al., 2019)	61.8	80.9	88.9	96.3	64.1	83.4	90.8	96.8	70.4	92.9	97.9	100.0
FILM (Gupta et al., 2020)	44.1	64.8	76.0	90.2	43.6	76.6	84.2	94.7	67.5	90.6	96.6	99.9
TreeGate (Zarpellon et al., 2021)	64.1	73.6	84.3	94.6	61.4	81.5	85.9	95.2	68.5	91.5	97.0	99.9
TGAT (Seyfi et al., 2023)	68.5	79.8	89.2	97.7	71.4	84.4	90.5	96.9	69.5	92.4	97.4	100.0
Symb4CO (Kuang et al., 2024a)	57.3	73.2	85.6	94.8	60.2	79.9	83.4	93.9	66.7	89.7	96.3	99.1
GS4CO (Kuang et al., 2024b)	56.8	72.7	87.2	94.5	61.5	81.4	85.7	94.3	67.1	90.9	95.7	99.4
CAMBranch (Lin et al., 2024)	60.7	78.6	87.4	96.2	63.5	82.7	90.5	96.8	68.9	91.2	96.8	99.9
MILP-Evolve (Li et al., 2025)	61.3	74.2	88.6	97.1	62.3	83.1	88.9	96.4	61.8	88.8	97.5	99.9
Ours	68.9	85.3	92.3	98.2	66.4	85.2	91.6	97.4	71.3	93.8	97.6	100.0
Ours	68.9	85.3	92.3	98.2	66.4	85.2	91.6	97.4	71.3	93.8	97.6	100.0

Table 3. Ablation study on the set covering problem.

Model	Accuracies (%)					Easy		Medium		Hard		
	acc@1↑	acc@1 (top 20%)↑	acc@3↑	acc@3 (top 20%)↑	acc@5↑	acc@5 (top 20%)↑	Time↓	Nodes↓	Time↓	Nodes↓	Time↓	Nodes↓
w/o UAMD	64.2	46.7	82.6	71.9	91.1	81.0	6.04	139	41.16	1479	1096.43	34461
w/o EquMD	64.8	47.2	83.4	72.2	91.2	81.3	6.04	136	40.85	1474	1073.76	33897
w/o PerMD	68.1	51.1	85	74.9	92.2	82.3	6.00	119	37.14	1457	975.31	29841
w/o DSCons	65.4	43.3	83.2	68.8	90.8	80.2	6.03	135	41.33	1473	1137.06	33580
w/o DSWeights	66.4	45.7	84.4	72.1	91	81.3	6.01	126	39.82	1467	1085.46	31478
w/o HBS	68.9	51.3	85.3	75.3	92.3	82.5	5.95	107	37.85	1467	1011.35	30258
Ours	68.9	51.3	85.3	75.3	92.3	82.5	5.99	117	37.01	1452	953.24	29375

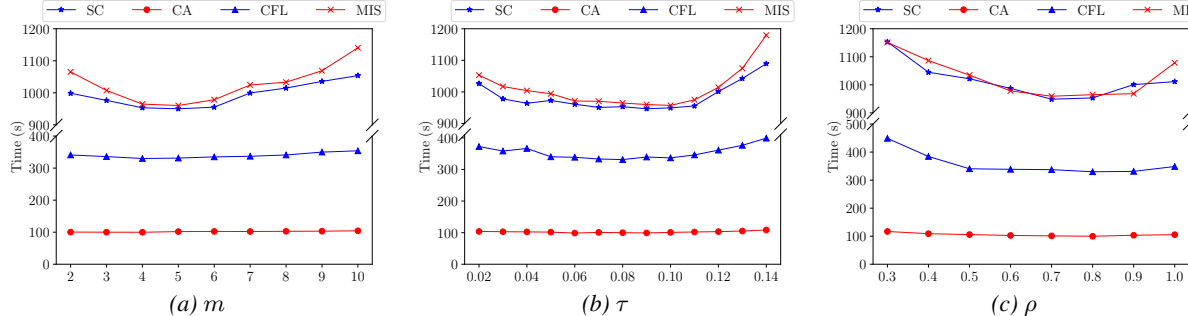


Figure 2. Parameter analysis. In each subplot, SC indicates Set Covering, CA indicates Combinatorial Auction, CFL indicates Capacitated Facility Location, and MIS indicates Maximum Independent Set.

achieving the most wins, validating both efficiency and generalization.

Exp-2: Performance on Branching Accuracy. We evaluate top- k ($k = 1, 3, 5, 10$) branching accuracy against neural baselines based on strong branching, excluding FSB and RPB (non-learning) as well as T-BranT (not trained on strong branching), with results in Table 3. Our method achieves the best performance across all four problems, with average improvements over the current best-performing method TGAT of 0.4%, 5.1%, 4.0%, and 0.7% for acc@1, acc@3, acc@5, and acc@10, respectively. Notably, we aim to balance branching speed and accuracy, which motivates our use of GCNN rather than complex models like TGAT, complemented by optimizing training to improve accuracy. High acc@5 and acc@10 further indicate that top-ranked candidates reliably contain strong branching choices, motivating our hybrid branching strategy.

Exp-3: Ablation Study. We conduct an ablation study on the set covering problem to evaluate the contributions of Upstream-Augmented MILP Derivation (UAMD) and Dynamic Stratified Contrastive Learning (DSCons). We report acc@1, acc@3, and acc@5 for the top 20% shall-

low nodes (acc@1–5 top 20%) to assess upstream prediction quality. The results are shown in Table 3, where “w/o UAMD” and “w/o DSCons” denote SC-MILP without UAMD and DSCons, respectively, “w/o EquMD” and ‘w/o PerMD” denote SC-MILP without equivalent and perturbed MILP derivation, respectively, “w/o DSWeights” denotes contrastive learning without dynamic stratified weights and “w/o HBS” denotes branching without hybrid branching strategy.

Compared with the ablation variants, the full model achieves the highest accuracy, fastest solving time, and smallest B&B tree size in most cases, demonstrating the effectiveness and complementarity of each component. Removing UAMD increases solving time by 14.7% and decreases acc@1 by 4.7%, with the largest drop caused by omitting equivalent MILP derivation (w/o EquMD) and minimal effect from Perturbed MILP Derivation (w/o PerMD), highlighting the critical role of equivalent MILP derivation in upstream augmentation. Removing DSCons raises solving time by 18.9% and reduces acc@1 by 3.5%, while retaining contrastive learning without dynamic stratified weights (w/o DSWeights) partially recovers performance, emphasizing the importance

of dynamic stratified weighting. Removing HBS does not affect the intrinsic branching accuracy, as reflected by identical acc@k metrics. On easy instances, removing HBS slightly reduces solving time because acc@1 is already high and the extra computation from top-k strong branching outweighs its benefit. On medium and hard instances, HBS helps reduce solving time and explored nodes, although the gains are modest compared with our two main components.

Notably, accuracy drops for upstream nodes are more pronounced: “w/o ACons” and “w/o UAMD” cause additional 3.1% and 0.3% decreases compared with all nodes, confirming that our method particularly enhances predictions for the most critical upstream portion of the B&B tree, where accurate branching decisions have the greatest impact on overall solving efficiency.

Exp-4: Parameter Analysis. We evaluated the impact of three key hyperparameters: group number m , contrastive learning temperature τ , and variable ratio threshold ρ . We vary m from 2 to 10, τ from 0.02 to 0.14, and ρ from 0.3 to 1, while keeping other settings consistent with **Exp-1**. The range of τ follows the common setting (Khosla et al., 2020). The results are shown in Fig. 2. We can find that: 1) As shown in Fig. 2a, model performance first improves with increasing m but then declines as m continues to rise. This indicates an optimal trade-off between distinguishing diverse node features with more groups and avoiding overpartitioning, which may disrupt shared patterns among adjacent strata. Selecting m near this optimal range (4–6) is likely to maximize solving efficiency, in agreement with the results obtained using the elbow methods; 2) The solving efficiency with varying τ exhibits a similar trend as that of m (Fig. 2b). Low values of τ make the model overly sensitive to hard samples, leading to unstable training, while high values weaken the contrastive separability. An intermediate τ (0.08 to 0.1) thus provides a balance between training stability and feature discriminability, yielding the best overall performance; 3) The effect of ρ follows a comparable pattern (Fig. 2c). As ρ increases, more nodes are processed using the hybrid branching strategy, which refines branching decisions but also increases the computational cost at these nodes. Initially, the gain in accuracy outweighs the added computational cost; however, beyond a certain threshold (0.8 and 0.9), further increases in ρ yield diminishing returns in accuracy relative to the cost. This indicates the existence of an optimal trade-off point for ρ that maximizes solving efficiency.

6. Conclusion

In this paper, we propose *SC-MILP*, a Dynamic Stratified Contrastive Training framework for MILP branching. By grouping nodes according to feature distributions and generating both equivalent and perturbed upstream MILPs, *SC-*

MILP trains a discriminative model that encourages moderate separation between adjacent phases and stronger discrimination for distant phases through dynamic stratified contrastive learning. This effectively models fine-grained semantic differences across the B&B tree, enhances branching accuracy and solving efficiency. Experimental results demonstrate that *SC-MILP* achieves SOTA branching performance and reduces MILP solving time by an average of 12.36%. In the future, we plan to develop a neural model that generalizes across diverse MILP types, allowing it to handle a wider range of problem instances. Beyond the SCIP solver, we also aim to extend *SC-MILP* to multiple MILP solvers, further broadening its practical applicability.

References

Achterberg, T., Koch, T., and Martin, A. Branching rules revisited. *Operations Research Letters*, 33(1):42–54, 2005.

Alvarez, A. M., Louveaux, Q., and Wehenkel, L. A machine learning-based approximation of strong branching. *INFORMS Journal on Computing*, 29(1):185–195, 2017.

Applegate, D., Bixby, R., Chvátal, V., and Cook, W. Finding cuts in the tsp (a preliminary report). Technical report, Report, 1995.

Ashouri, A., Fux, S. S., Benz, M. J., and Guzzella, L. Optimal design and operation of building services using mixed-integer linear programming techniques. *Energy*, 59:365–376, 2013.

Balas, E. and Ho, A. Set covering algorithms using cutting planes, heuristics, and subgradient optimization: a computational study. In *Combinatorial optimization*. 2009.

Bellabdaoui, A. and Teghem, J. A mixed-integer linear programming model for the continuous casting planning. *International Journal of Production Economics*, 104(2):260–270, 2006.

Bénichou, M., Gauthier, J.-M., Girodet, P., Hentges, G., Ribière, G., and Vincent, O. Experiments in mixed-integer linear programming. *Mathematical programming*, 1(1):76–94, 1971.

Bergman, D., Cire, A. A., Van Hoeve, W.-J., and Hooker, J. *Decision diagrams for optimization*, volume 1. Springer, 2016.

Burges, C. J. From ranknet to lambdarank to lambdamart: An overview. *Learning*, 11(23-581):81, 2010.

Chen, Z., Liu, J., Chen, X., Wang, W., and Yin, W. Rethinking the capacity of graph neural networks for branching strategy. In *Advances in neural information processing systems*, 2024.

Cornuéjols, G., Sridharan, R., and Thizy, J.-M. A comparison of heuristics and relaxations for the capacitated plant location problem. *European journal of operational research*, 50(3):280–297, 1991.

Etheve, M., Alès, Z., Bissuel, C., Juan, O., and Kedad-Sidhoum, S. Reinforcement learning for variable selection in a branch and bound algorithm. In *International conference on integration of constraint programming, artificial intelligence, and operations research*, 2020.

Feng, S. and Yang, Y. Sorrel: Suboptimal-demonstration-guided reinforcement learning for learning to branch. In *Proceedings of the AAAI Conference on Artificial Intelligence*, volume 39, pp. 11212–11220, 2025.

Fischetti, M. and Lodi, A. Local branching. *Mathematical programming*, 98(1):23–47, 2003.

Floudas, C. A. and Lin, X. Mixed integer linear programming in process scheduling: Modeling, algorithms, and applications. *Annals of Operations Research*, 139(1):131–162, 2005.

Gao, Y., Ma, L., Yu, Z., Zhang, S., Fang, J., Gao, X., and Chen, G. Lightweight gcn encoder and sequential decoder for multi-candidate carpooling route planning in road network. In *Proceedings of the ACM Web Conference 2024*, 2024.

Gasse, M., Chételat, D., Ferroni, N., Charlin, L., and Lodi, A. Exact combinatorial optimization with graph convolutional neural networks. In *Advances in neural information processing systems*, 2019.

Godart, A., Manier, H., Bloch, C., and Manier, M.-A. Milp for a variant of pickup & delivery problem for both passengers and goods transportation. In *IEEE International Conference on Systems, Man and Cybernetics*, 2018.

Guo, W., Wang, R., Xu, Y., and Jin, Y. Unified and generalizable reinforcement learning for facility location problems on graphs. In *Proceedings of the ACM Web Conference 2025*, 2025.

Gupta, P., Gasse, M., Khalil, E., Mudigonda, P., Lodi, A., and Bengio, Y. Hybrid models for learning to branch. In *Advances in neural information processing systems*, 2020.

Huang, T., Ferber, A. M., Zharmagambetov, A., Tian, Y., and Dilkina, B. Contrastive predict-and-search for mixed integer linear programs. In *Forty-first International Conference on Machine Learning*, 2024.

Khalil, E., Le Bodic, P., Song, L., Nemhauser, G., and Dilkina, B. Learning to branch in mixed integer programming. In *Proceedings of the AAAI conference on artificial intelligence*, 2016.

Khalil, E. B., Morris, C., and Lodi, A. Mip-gnn: A data-driven framework for guiding combinatorial solvers. In *Proceedings of the AAAI conference on artificial intelligence*, 2022.

Khosla, P., Teterwak, P., Wang, C., Sarna, A., Tian, Y., Isola, P., Maschinot, A., Liu, C., and Krishnan, D. Supervised contrastive learning. In *Advances in neural information processing systems*, 2020.

Kuang, Y., Wang, J., Liu, H., Zhu, F., Li, X., Zeng, J., Hao, J., Li, B., and Wu, F. Rethinking branching on exact combinatorial optimization solver: The first deep symbolic discovery framework. In *The Twelfth International Conference on Learning Representations*, 2024a.

Kuang, Y., Wang, J., Zhou, Y., Li, X., Zhu, F., Hao, J., and Wu, F. Towards general algorithm discovery for combinatorial optimization: Learning symbolic branching policy from bipartite graph. In *Forty-first International Conference on Machine Learning*, 2024b.

Land, A. and Doig, A. An automatic method of solving discrete programming problems. *Econometrica: Journal of the Econometric Society*, pp. 497–520, 1960.

Leyton-Brown, K., Pearson, M., and Shoham, Y. Towards a universal test suite for combinatorial auction algorithms. In *Proceedings of the 2nd ACM conference on Electronic commerce*, 2000.

Li, S., Kulkarni, J., Menache, I., Wu, C., and Li, B. Towards foundation models for mixed integer linear programming. In *ICLR*, 2025.

Lin, J., Zhu, J., Wang, H., and Zhang, T. Learning to branch with tree-aware branching transformers. *Knowledge-Based Systems*, 252:109455, 2022.

Lin, J., Meng, X., Xiong, Z., and Wang, H. Cambranch: Contrastive learning with augmented milps for branching. In *The Twelfth International Conference on Learning Representations*, 2024.

Liu, J., Zhou, M., Ma, S., and Pan, L. Mata*: Combining learnable node matching with a* algorithm for approximate graph edit distance computation. In *CIKM*, pp. 1503–1512, 2023.

Marcos Alvarez, A., Louveaux, Q., and Wehenkel, L. A supervised machine learning approach to variable branching in branch-and-bound. Technical report, Report, 2014.

Parsonson, C. W., Laterre, A., and Barrett, T. D. Reinforcement learning for branch-and-bound optimisation using retrospective trajectories. In *Proceedings of the AAAI conference on artificial intelligence*, 2023.

Pei, Q. and Chen, S.-J. Learn branching policies with an attention-based model. *Procedia Computer Science*, 221: 1416–1422, 2023.

Scavuzzo, L., Chen, F., Chételat, D., Gasse, M., Lodi, A., Yorke-Smith, N., and Aardal, K. Learning to branch with tree mdps. In *Advances in neural information processing systems*, 2022.

Seyfi, M., Banitalebi-Dehkordi, A., Zhou, Z., and Zhang, Y. Exact combinatorial optimization with temporally attentional graph neural networks. In *Joint European Conference on Machine Learning and Knowledge Discovery in Databases*, 2023.

Soylu, A., Oruç, C., Turkay, M., Fujita, K., and Asakura, T. Synergy analysis of collaborative supply chain management in energy systems using multi-period milp. *European Journal of Operational Research*, 174(1):387–403, 2006.

Vielma, J. P. Mixed integer linear programming formulation techniques. *Siam Review*, 57(1):3–57, 2015.

Wang, F. and Li, B. Fair surveillance assignment problem. In *Proceedings of the ACM Web Conference 2024*, 2024.

Wang, J., Wang, Z., Li, X., Kuang, Y., Shi, Z., Zhu, F., Yuan, M., Zeng, J., Zhang, Y., and Wu, F. Learning to cut via hierarchical sequence/set model for efficient mixed-integer programming. *IEEE Transactions on Pattern Analysis and Machine Intelligence*, 2024.

Yan, H., Tan, H., Wang, H., Zhang, D., and Yang, Y. Robust route planning under uncertain pickup requests for last-mile delivery. In *Proceedings of the ACM Web Conference 2024*, 2024.

Zarpellon, G., Jo, J., Lodi, A., and Bengio, Y. Parameterizing branch-and-bound search trees to learn branching policies. In *Proceedings of the AAAI conference on artificial intelligence*, 2021.

Zhang, T., Banitalebi-Dehkordi, A., and Zhang, Y. Deep reinforcement learning for exact combinatorial optimization: Learning to branch. In *26th international conference on pattern recognition*, 2022.

Zhao, P., Zhou, Y., Wang, D., Cao, Z., Xiao, Y., Wu, X., Li, Y., Liu, H., Du, W., Jiang, Y., et al. Dual operation aggregation graph neural networks for solving flexible job-shop scheduling problem with reinforcement learning. In *Proceedings of the ACM Web Conference 2025*, 2025.

A. Branch-and-Bound Framework

The *Branch-and-Bound* (B&B) algorithm is the core framework of modern MILP solvers. It maintains a search tree where:

(1)

- Each node represents a subproblem obtained from (1) by adding branching constraints.
- The LP relaxation of the subproblem provides a lower bound on its objective value.
- Nodes are *branched* if their LP solution is fractional, *pruned* if their bound is worse than the incumbent, or used to update the incumbent if feasible and better.

B&B is exact: once all nodes are processed or pruned, the best incumbent is the global optimum.

B. Strong Branching

A key component of B&B is the *branching strategy*, i.e., how to choose the variable to branch on. *Strong Branching* (SB) is one of the most effective rules: for each fractional candidate variable x_j with LP value x_j^* , SB tentatively branches by adding:

$$x_j \leq \lfloor x_j^* \rfloor \quad \text{and} \quad x_j \geq \lceil x_j^* \rceil, \quad (10)$$

and solves the LP relaxation for each branch. Let z^* denote the LP bound of the current node, and z_j^\downarrow and z_j^\uparrow denote the LP bounds obtained from the down and up branches, respectively. The *bound improvements* are defined as:

$$\Delta_j^\downarrow = z_j^\downarrow - z^*, \quad \Delta_j^\uparrow = z_j^\uparrow - z^*, \quad (11)$$

where $\Delta_j^\downarrow > 0$ (or $\Delta_j^\uparrow > 0$) indicates that the corresponding branch yields a tighter bound, thereby potentially enabling more pruning in subsequent search. The SB score for variable x_j is computed as:

$$s_j = \Delta_j^\downarrow + \Delta_j^\uparrow, \quad (12)$$

and the variable with the highest s_j is selected. While SB often yields smaller search trees, it requires solving $2n$ additional LPs for n candidates, making it computationally expensive.

C. Proofs

Proof of Theorem 4.2. (1) *Feasible-Domain Correspondence.* Since T is invertible, $\phi(\mathbf{x}) = T\mathbf{x} + \mathbf{t}$ is a bijection on \mathbb{R}^n with inverse $\phi^{-1}(\hat{\mathbf{x}}) = T^{-1}(\hat{\mathbf{x}} - \mathbf{t})$. If $\mathbf{x} \in \mathcal{P}$, then:

$$A\mathbf{x} \leq \mathbf{b} \iff AT^{-1}(\hat{\mathbf{x}} - \mathbf{t}) \leq \mathbf{b} \iff \hat{A}\hat{\mathbf{x}} \leq \hat{\mathbf{b}},$$

The bound constraints $\mathbf{l} \leq \mathbf{x} \leq \mathbf{u}$ transform similarly into $\hat{\mathbf{l}} \leq \hat{\mathbf{x}} \leq \hat{\mathbf{u}}$. Thus $\mathbf{x} \in \mathcal{P} \iff \hat{\mathbf{x}} = \phi(\mathbf{x}) \in \hat{\mathcal{P}}$, proving the bijection between feasible domains.

(2) *Optimal-Solution Correspondence.* Let the original LP objective be $f(\mathbf{x}) = \mathbf{c}^\top \mathbf{x}$ and the transformed LP objective be

$$\hat{f}(\hat{\mathbf{x}}) = \hat{\mathbf{c}}^\top \hat{\mathbf{x}} + \gamma, \quad \text{where} \quad \hat{\mathbf{c}} = (T^{-1})^\top \mathbf{c}, \quad \gamma = -\mathbf{c}^\top T^{-1} \mathbf{t}.$$

Then for any $\mathbf{x} \in \mathcal{P}$ and $\hat{\mathbf{x}} = \phi(\mathbf{x})$,

$$\hat{f}(\hat{\mathbf{x}}) = \mathbf{c}^\top \mathbf{x}.$$

Suppose \mathbf{x}^* is optimal for the original LP, but $\hat{\mathbf{x}}^* = \phi(\mathbf{x}^*)$ is not optimal for the transformed LP. Then there exists $\hat{\mathbf{x}} \in \hat{\mathcal{P}}$ such that $\hat{f}(\hat{\mathbf{x}}) < \hat{f}(\hat{\mathbf{x}}^*)$. Let $\mathbf{x} = \phi^{-1}(\hat{\mathbf{x}}) \in \mathcal{P}$. By the objective equality, $\mathbf{c}^\top \mathbf{x} < \mathbf{c}^\top \mathbf{x}^*$, contradicting the optimality of \mathbf{x}^* . The converse direction follows symmetrically. Therefore, the optimal solution sets correspond bijectively under ϕ . \square

Proof of Theorem 4.3. Let $f(\mathbf{x}) = \mathbf{c}^\top \mathbf{x}$ be the original objective, and $\hat{f}(\hat{\mathbf{x}}) = \hat{\mathbf{c}}^\top \hat{\mathbf{x}} + \gamma$ be the transformed objective with $\hat{\mathbf{c}} = (T^{-1})^\top \mathbf{c}$ and $\gamma = -\mathbf{c}^\top T^{-1} \mathbf{t}$.

Let \mathbf{x}^* be the optimal solution of the original LP, and let $\hat{\mathbf{x}}^* = T\mathbf{x}^* + \mathbf{t}$ be the corresponding optimal solution of the transformed LP. Then the optimal objective values are equal:

$$f(\mathbf{x}^*) = \hat{f}(\hat{\mathbf{x}}^*).$$

For strong branching on variable x_j , consider the two subproblems formed by adding branching constraints:

$$\mathcal{P}_j^\downarrow := \{\mathbf{x} \in \mathcal{P} \mid x_j \leq \lfloor x_j^* \rfloor\}, \quad \mathcal{P}_j^\uparrow := \{\mathbf{x} \in \mathcal{P} \mid x_j \geq \lceil x_j^* \rceil\}.$$

Under the variable transformation, these constraints correspond to

$$\hat{x}_{\pi(j)} \leq \lfloor \hat{x}_{\pi(j)}^* \rfloor, \quad \hat{x}_{\pi(j)} \geq \lceil \hat{x}_{\pi(j)}^* \rceil,$$

where $\pi(j)$ is the index of the variable in $\hat{\mathbf{x}}$ corresponding to x_j .

Thus, the transformed subproblems are:

$$\begin{aligned} \hat{\mathcal{P}}_{\pi(j)}^\downarrow &:= \{\hat{\mathbf{x}} \in \hat{\mathcal{P}} \mid \hat{x}_{\pi(j)} \leq \lfloor \hat{x}_{\pi(j)}^* \rfloor\}, \\ \hat{\mathcal{P}}_{\pi(j)}^\uparrow &:= \{\hat{\mathbf{x}} \in \hat{\mathcal{P}} \mid \hat{x}_{\pi(j)} \geq \lceil \hat{x}_{\pi(j)}^* \rceil\}. \end{aligned}$$

Since the original and transformed feasible regions are bijectively related by

$$\hat{\mathbf{x}} = T\mathbf{x} + \mathbf{t}, \quad \mathbf{x} = T^{-1}(\hat{\mathbf{x}} - \mathbf{t}),$$

we have a one-to-one correspondence between \mathcal{P}_j^\downarrow and $\hat{\mathcal{P}}_{\pi(j)}^\downarrow$, and between \mathcal{P}_j^\uparrow and $\hat{\mathcal{P}}_{\pi(j)}^\uparrow$.

Moreover, the objectives satisfy

$$\hat{f}(\hat{\mathbf{x}}) = f(\mathbf{x}), \quad \forall \hat{\mathbf{x}} \in \hat{\mathcal{P}}, \mathbf{x} = T^{-1}(\hat{\mathbf{x}} - \mathbf{t}).$$

Let the optimal LP values for the subproblems be

$$z_j^\downarrow := \min_{\mathbf{x} \in \mathcal{P}} f(\mathbf{x}), \quad \hat{z}_{\pi(j)}^\downarrow := \min_{\hat{\mathbf{x}} \in \hat{\mathcal{P}}} \hat{f}(\hat{\mathbf{x}}).$$

Since the feasible regions and objectives correspond exactly,

$$z_j^\downarrow = \hat{z}_{\pi(j)}^\downarrow.$$

Similarly,

$$z_j^\uparrow = \hat{z}_{\pi(j)}^\uparrow.$$

Define the strong branching scores (bound improvements) by

$$\Delta_j^\downarrow = z_j^\downarrow - z^*, \quad \Delta_j^\uparrow = z_j^\uparrow - z^*,$$

and

$$\hat{\Delta}_{\pi(j)}^\downarrow = \hat{z}_{\pi(j)}^\downarrow - \hat{z}^*, \quad \hat{\Delta}_{\pi(j)}^\uparrow = \hat{z}_{\pi(j)}^\uparrow - \hat{z}^*,$$

where $z^* = f(\mathbf{x}^*)$ and $\hat{z}^* = \hat{f}(\hat{\mathbf{x}}^*)$.

Because $z^* = \hat{z}^*$ and $z_j^\downarrow = \hat{z}_{\pi(j)}^\downarrow$, $z_j^\uparrow = \hat{z}_{\pi(j)}^\uparrow$, it follows that

$$\Delta_j^\downarrow = \hat{\Delta}_{\pi(j)}^\downarrow, \quad \Delta_j^\uparrow = \hat{\Delta}_{\pi(j)}^\uparrow.$$

Since strong branching selects the branching variable and direction based on these scores, the decision for x_j in the original problem corresponds exactly to the decision for $\hat{x}_{\pi(j)}$ in the transformed problem. \square

Proof of Theorem 4.4. (1) **Bijection of feasible regions.** Since B and D are invertible, T is invertible with

$$T^{-1} = \begin{pmatrix} B^{-1} & 0 \\ -D^{-1}FB^{-1} & D^{-1} \end{pmatrix}.$$

The affine transformation $\phi(\mathbf{x}) = T\mathbf{x} + \mathbf{t}$, therefore, has the inverse

$$\phi^{-1}(\hat{\mathbf{x}}) = T^{-1}(\hat{\mathbf{x}} - \mathbf{t}),$$

so ϕ is bijective on \mathbb{R}^n . By construction, the transformed MILP is obtained from the original one by substituting $\mathbf{x} = T^{-1}(\hat{\mathbf{x}} - \mathbf{t})$ into all constraints. Hence \mathbf{x} is feasible for the original MILP if and only if $\hat{\mathbf{x}} = \phi(\mathbf{x})$ is feasible for the transformed MILP.

(2) **Preservation of integrality.** For the integer block, we have

$$\hat{\mathbf{x}}_{\mathcal{I}} = B\mathbf{x}_{\mathcal{I}} + \mathbf{t}_{\mathcal{I}}.$$

Because B is a signed permutation matrix, $B\mathbf{z} \in \mathbb{Z}^k$ for all $\mathbf{z} \in \mathbb{Z}^k$. With $\mathbf{t}_{\mathcal{I}} \in \mathbb{Z}^k$, it follows that $\mathbf{x}_{\mathcal{I}} \in \mathbb{Z}^k \implies \hat{\mathbf{x}}_{\mathcal{I}} \in \mathbb{Z}^k$. Conversely, if $\hat{\mathbf{x}}_{\mathcal{I}} \in \mathbb{Z}^k$ then

$$\mathbf{x}_{\mathcal{I}} = B^{-1}(\hat{\mathbf{x}}_{\mathcal{I}} - \mathbf{t}_{\mathcal{I}}) \in \mathbb{Z}^k$$

because B^{-1} is also a signed permutation matrix.

(3) **Correspondence of optimal solutions.** Let the original MILP objective be $f(\mathbf{x}) = \mathbf{c}^T \mathbf{x}$. Define the transformed objective as

$$\hat{f}(\hat{\mathbf{x}}) = \hat{\mathbf{c}}^T \hat{\mathbf{x}} + \gamma, \quad \hat{\mathbf{c}} = (T^{-1})^T \mathbf{c}, \quad \gamma = -\mathbf{c}^T T^{-1} \mathbf{t}.$$

Then for all \mathbf{x} and $\hat{\mathbf{x}} = \phi(\mathbf{x})$ we have $\hat{f}(\hat{\mathbf{x}}) = f(\mathbf{x})$. If \mathbf{x}^* is optimal for the original MILP, $\hat{\mathbf{x}}^* = \phi(\mathbf{x}^*)$ is feasible for the transformed MILP with the same objective value. If $\hat{\mathbf{x}}^*$ were not optimal, there would exist $\hat{\mathbf{y}}$ feasible with $\hat{f}(\hat{\mathbf{y}}) < \hat{f}(\hat{\mathbf{x}}^*)$, implying that $\mathbf{y} = \phi^{-1}(\hat{\mathbf{y}})$ is feasible for the original MILP with $f(\mathbf{y}) < f(\mathbf{x}^*)$, contradicting optimality. The reverse direction is identical. Thus, optimal solutions correspond one-to-one. \square

D. Details of Upstream-Augmentation

D.1. Bipartite Graph Vertex Features

Following Gasse et al. (2019), we model the MILP corresponding to each node in the Branch-and-Bound (B&B) tree with a bipartite graph, denoted by $(\mathcal{G}, \mathcal{C}, \mathcal{E}, \mathcal{V})$, where the details of these features are shown in Table 4.

Table 4. An overview of the features for constraints, edges, and variables in the bipartite graph $s_i = (\mathcal{G}, \mathcal{C}, \mathcal{E}, \mathcal{V})$ following Gasse et al. (2019). \mathcal{C} = constraint vertex, \mathcal{E} = edge, \mathcal{V} = variable vertex.

Type	Feature	Description
C	obj.cos_sim	Cosine similarity between constraint and objective coefficients.
	bias	Normalized right-hand side (RHS) value.
	is.tight	Indicator of whether constraint is tight in LP solution.
	dualsol.val	Normalized dual value of the constraint.
E	age	LP age since last improvement on the current vertex.
	coef	Normalized coefficient a_{ij} linking variable x_j to constraint c_i .
V	type	One-hot encoding for variable type (binary variables, integer variables, implicit integer variables, and continuous variables).
	coef	Normalized objective coefficient c_j .
	has_lb / _ub	Indicator whether variable has lower/upper bounds.
	sol.is.at_lb / _ub	Indicator whether LP solution is at lower/upper bound.
	sol.frac	Fractionality of LP solution value.
	basis_status	One-hot simplex basis status: basic, upper, lower, zero.
	reduced_cost	Normalized reduced cost.
	age	LP age of the variable.
	sol_val	LP solution value of the variable.
inc_val / avg_inc_val		Value/Average value in the incumbent solutions

D.2. Graph Features of LT-MILP

The relationships between MILP and LT-MILP vertex features are illustrated in Table 5.

Specifically, consider the linear transformation

$$\hat{\mathbf{x}} = \phi(\mathbf{x}) = T\mathbf{x} + \mathbf{t},$$

where T is a diagonal matrix with entries ± 1 , and $\mathbf{t}_{\mathcal{I}} \in \mathbb{Z}^k$. Let the original LP relaxation of MILP (1) be

$$\min_{\mathbf{x}} \mathbf{c}^T \mathbf{x} \quad \text{s.t.} \quad A\mathbf{x} \leq \mathbf{b}, \quad \mathbf{l} \leq \mathbf{x} \leq \mathbf{u}.$$

Table 5. Relationship between MILP and *LT-MILP* vertex features. The notation $\mathbb{B} \leftrightarrow \mathbb{Z}$ denotes the potential mutual conversion between binary variables and integer variables.

Vertex feature	MILP	LT-MILP
Constraint vertex features (constraint i)		
obj_cos_sim	$C_{i,1}$	$C_{i,1}$
bias	$C_{i,2}$	$C_{i,2} + a_i^\top t / \ a_i\ $
is_tight	$C_{i,3}$	$C_{i,3}$
dualsol_val	$C_{i,4}$	$C_{i,4}$
age	$C_{i,5}$	$C_{i,5}$
Edge features (edge (i, j) of constraint i and variable j)		
coef	$E_{i,j}$	$T_{jj}E_{i,j}$
Variable vertex features (variable j)		
type	$V_{j,1}$	$V_{j,1}$ or $\mathbb{B} \leftrightarrow \mathbb{Z}$
coef	$V_{j,2}$	$T_{jj}V_{j,2}$
has_lb	$V_{j,3}$	if $T_{jj} = 1$, $V_{j,3}$, else $V_{j,4}$
has_ub	$V_{j,4}$	if $T_{jj} = 1$, $V_{j,4}$, else $V_{j,3}$
sol_is_at_lb	$V_{j,5}$	if $T_{jj} = 1$, $V_{j,5}$, else $V_{j,6}$
sol_is_at_ub	$V_{j,6}$	if $T_{jj} = 1$, $V_{j,6}$, else $V_{j,5}$
sol_frac	$V_{j,7}$	if $T_{jj} = 1$, $V_{j,7}$, else $1 - V_{j,7} \pmod{1}$
basis_status	$V_{j,8}$	$V_{j,8}$
reduced_cost	$V_{j,9}$	$T_{jj}V_{j,9}$
age	$V_{j,10}$	$V_{j,10}$
sol_val	$V_{j,11}$	$T_{jj}V_{j,11} + t_j$
inc_val	$V_{j,12}$	$T_{jj}V_{j,12} + t_j$
avg_inc_val	$V_{j,13}$	$T_{jj}V_{j,13} + t_j$

After the transformation, the LP becomes

$$\min_{\hat{\mathbf{x}}} \hat{\mathbf{c}}^\top \hat{\mathbf{x}} \quad \text{s.t.} \quad \hat{A}\hat{\mathbf{x}} \leq \hat{\mathbf{b}}, \hat{\mathbf{l}} \leq \hat{\mathbf{x}} \leq \hat{\mathbf{u}},$$

with $\hat{\mathbf{c}} = T^\top \mathbf{c}$, $\hat{A} = AT$, $\hat{\mathbf{b}} = \mathbf{b} + AT\mathbf{t}$, $\hat{\mathbf{l}} = T\mathbf{l} + \mathbf{t}$, $\hat{\mathbf{u}} = T\mathbf{u} + \mathbf{t}$.

Dual Solution Value (dualsol_val). Let \mathbf{y} denote the dual variables corresponding to $A\mathbf{x} \leq \mathbf{b}$. The dual LP is

$$\max_{\mathbf{y} \geq 0} \mathbf{b}^\top \mathbf{y} \quad \text{s.t.} \quad A^\top \mathbf{y} + \mathbf{s} = \mathbf{c}, \mathbf{s} \geq 0,$$

where \mathbf{s} are slack variables for bounds.

After transformation, the dual variables $\hat{\mathbf{y}}$ satisfy

$$\hat{A}^\top \hat{\mathbf{y}} + \hat{\mathbf{s}} = \hat{\mathbf{c}} \quad \Rightarrow \quad (AT)^\top \hat{\mathbf{y}} + \hat{\mathbf{s}} = T^\top \mathbf{c}.$$

Since T is diagonal with ± 1 , we have

$$A^\top \hat{\mathbf{y}} + T\hat{\mathbf{s}} = \mathbf{c}.$$

Comparing with the original dual, if we set

$$\hat{\mathbf{y}} = \mathbf{y}, \quad \hat{\mathbf{s}} = T\mathbf{s},$$

the dual feasibility is preserved.

Thus, the dual solution value for each constraint is preserved.

Fractionality of LP Solution (sol_frac). Consider an integer variable $x_j \in \mathcal{I}$ and its fractionality

$$\text{sol_frac}_j = \text{frac}(x_j),$$

where $\text{frac}(\cdot)$ denotes the fractional part.

After the linear transformation

$$\hat{x}_j = T_{jj}x_j + t_j, \quad T_{jj} \in \{+1, -1\}, \quad t_j \in \mathbb{Z},$$

the fractionality becomes

$$\text{sol_frac}_j = \text{frac}(\hat{x}_j) = \text{frac}(T_{jj}x_j + t_j).$$

Since adding an integer t_j does not change the fractional part, we have

$$\text{sol_frac}_j = \text{frac}(T_{jj}x_j).$$

Now consider the two cases for T_{jj} :

- $T_{jj} = +1$: $\text{sol_frac}_j = \text{frac}(x_j) = \text{sol_frac}_j$. The fractionality remains unchanged.
- $T_{jj} = -1$: $\text{sol_frac}_j = \text{frac}(-x_j)$. Recall that

$$\text{frac}(-x_j) = \begin{cases} 0, & \text{if } \text{frac}(x_j) = 0, \\ 1 - \text{frac}(x_j), & \text{otherwise.} \end{cases}$$

In summary, the transformed fractionality can be expressed as

$$\text{sol_frac}_j = \begin{cases} \text{sol_frac}_j, & T_{jj} = +1, \\ 1 - \text{sol_frac}_j \pmod{1}, & T_{jj} = -1. \end{cases}$$

Reduced Cost (reduced_cost). Original reduced cost:

$$r_j = c_j - A_{:,j}^\top \mathbf{y}.$$

where $A_{:,j}$ is the j -th column of the constraint matrix, and \mathbf{y} denotes the dual vector of the constraints.

After transformation,

$$\hat{r}_j = \hat{c}_j - \hat{A}_{:,j}^\top \hat{\mathbf{y}} = T_{jj}c_j - (AT)_{:,j}^\top \mathbf{y} = T_{jj}(c_j - A_{:,j}^\top \mathbf{y}) = T_{jj}r_j.$$

Therefore, `reduced_cost` flips sign if $T_{jj} = -1$ and remains the same if $T_{jj} = 1$.

Bounds-Related Features. The features `has_lb` and `has_ub` are binary indicators of whether a variable has finite lower and upper bounds, respectively. Similarly, `sol_is_at_lb` (`sol_is_at_ub`) indicates whether the LP solution of a variable coincides with its lower (upper) bound.

Under the transformation $\hat{x}_j = T_{jj}x_j + t_j$, the new bounds are given by $\hat{l}_j = T_{jj}l_j + t_j$, $\hat{u}_j = T_{jj}u_j + t_j$. Since the existence of finite bounds is preserved by affine transformations, the values of `has_lb` and `has_ub` remain unchanged. However, the identity of active bounds may switch when $T_{jj} = -1$: if the solution was originally at l_j , after transformation it corresponds to \hat{u}_j , and vice versa for u_j .

Solution-Related Features. The feature `sol_val` records the LP solution value of a variable, while `inc_val` and `avg_inc_val` represent the variable's value in the current incumbent solution and the average value across all incumbent solutions, respectively.

Under the linear transformation $\hat{x}_j = T_{jj}x_j + t_j$, these values transform consistently as

$$\begin{aligned} \text{sol_val}_j &= T_{jj} \cdot \text{sol_val}_j + t_j, & \text{inc_val}_j &= T_{jj} \cdot \text{inc_val}_j + t_j, \\ \text{avg_inc_val}_j &= T_{jj} \cdot \text{avg_inc_val}_j + t_j. \end{aligned}$$

Therefore, these features undergo the same affine transformation as the variables themselves.

D.3. Graph Features of *RC-MILP*

After augmenting the MILP with a redundant constraint $a_r^\top x \leq b_r$, a new constraint vertex is added to \mathcal{G} while other vertices' features remain unchanged.

Constraint Vertex features. For the newly added vertex, its features such as `obj.cos_sim` and `bias` are computed from a_r and b_r , while `is_tight` and `dualsol_val` are set to zero, since the redundant constraint does not affect the optimal solution boundary and re-solving the LP will not make it tight. `age` is also set to zero.

Edge features. The newly added vertex is connected to variable vertices with nonzero coefficients in a_r , with `coef` reflecting the normalized values.